Computers and Geotechnics 134 (2021) 104140

Contents lists available at ScienceDirect

Computers and Geotechnics

journal homepage: www.elsevier.com/locate/compgeo

Research Paper

A framework for the design of vertically loaded piles in spatially variable soil

Yongmin Cai [a], Fraser Bransby [a], Christophe Gaudin [a,*], Marco Uzielli [b,c]

[a] Centre for Offshore Foundation Systems and Oceans Graduate School, The University of Western Australia, Perth 6009, Australia
[b] University of Florence, Italy
[c] Georisk Engineering S.r.l, Italy

ARTICLE INFO

Keywords:
Risk and probability analysis
Pile capacity
Reliability
Spatial variability

ABSTRACT

Each pile in an offshore wind farm may be designed solely on the results of a single cone penetration test (CPT) positioned at its center or based on sample statistics calculated from multiple investigated locations in the same geotechnical unit. This study investigates quantitatively the effects of spatial variability of soil on the efficacy of the two approaches to achieve a reliable design. Random field theory is used to generate sets of cone tip resistance profiles with different characteristics to represent different seabed conditions and piles are 'designed' using the above two approaches and the partial factor method to withstand a given vertical drained design load distribution. The effects of the inaccuracies in prediction of pile capacity from the CPT data are quantified in terms of the scatter in calculated reliability (or probability of failure). Outputs of the parametric statistical analysis demonstrate that the ability of the two CPT-based approaches to produce a reliable foundation design is dependent on the ratio between the horizontal scale of fluctuation and the pile diameter, and the overall variability (coefficient of variation) of the seabed properties. Modifications to deterministic, partial factor design approaches are suggested to account for these uncertainties to ensure target reliabilities are achieved.

1. Introduction

Piles are utilized increasingly for bottom supported and floating offshore infrastructure for both renewables and oil and gas applications (Salgado and Lee, 1999; ISO, 2020; API, 2014; Wu et al., 2019). Although there are still some level of uncertainties in quantifying piles' axial (e.g. Lehane et al., 2017) and lateral response (e.g. Klinkvort, 2012; Byrne et al., 2015; Thieken et al., 2015) for a given site condition, it is likely that larger cost savings can be achieved by considering more carefully the derivation of site-specific inputs into design methodologies (Phoon and Kulhawy, 1999; Kallehave et al., 2015; Cai et al., 2019; Li et al., 2019).

Site-specific pile design is based on information from geotechnical and geophysical surveys, and seabed parameters are conventionally selected assuming spatially homogeneous soil at each pile location (i.e. without consideration of spatial variation in properties within each pile 'footprint'). This means that if a pile-specific cone penetration test (CPT) is conducted in the planned pile location, then the pile response is normally calculated deterministically using the location-specific CPT data (and supporting sample testing results) without considering further how soil properties may vary laterally in the zone of influence of the pile (or pile group). Alternatively, if the pile is to be constructed away from investigated locations, then the pile response is likely to be determined based on the statistics of the obtained geotechnical data in the same geotechnical unit (as identified by collating and comparing geotechnical data and using geophysical data to confirm similarity of geological conditions). This may be done by selecting a characteristic (or design) line based on a specified quantile of the data for the limit state of interest (Phoon and Kulhawy, 1999; Uzielli et al., 2007; 2019;; Uzielli and Mayne, 2019) and using this in standard deterministic (partial factor or global factor of safety) design.

At present, large diameter piles are being installed to support increasingly large offshore infrastructure (e.g. 7.8 m diameter monopiles for the Veja Mate offshore wind facilities (Negro et al., 2017)) and, although normally smaller, anchor piles may be as large as 5.5 m in diameter (e.g. Erbrich et al., 2017; Dechiron et al., 2020). Consequently, the distribution of soil strength within the pile footprint (which will govern pile response) may be different to that derived from the pile-specific CPT data (e.g. Fig. 1) or the statistics of the collated unit-specific data. Current studies about evaluating the effect of this

* Corresponding author.
E-mail address: christophe.gaudin@uwa.edu.au (C. Gaudin).

https://doi.org/10.1016/j.compgeo.2021.104140

Available online 31 March 2021

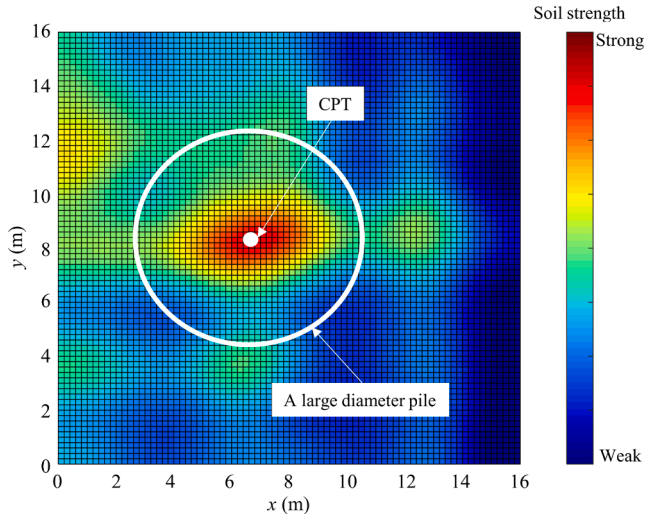

Fig. 1. A horizontal soil profile with variability of soil strength.

uncertainty on pile design are scarce, and large factors of safety or large partial factors and/or conservative characteristic lines are often used to ensure safe design. It is uncertain currently whether this may result in over-engineered and thereby less economic piles.

In light of the above uncertainty, the paper investigates how the reliability (and designed size) of large diameter piles in sand are affected by the method of selection of the characteristic design profile, how this reliability depends on the variability of the soil properties and consequently how, more generally adopted, deterministic design approaches (e.g. using partial factors) can be modified to ensure target reliabilities are achieved. In order to identify trends in data and to suggest a design framework this process is implemented for a limited sub-set of parameters in design space (and only for drained uplift loading as relevant for an anchor pile for wave energy converter for instance). The paper investigates two common design scenarios ((i) when the designer has data from a single CPT at the pile location, and (ii) when unitized CPT data is available) providing recommendations for each.

The investigation was conducted using numerical analyses and random field theory, with the use of Monte Carlo simulation. Three-dimensional (3D) random fields of net cone tip resistance (q_c) were generated for different scenarios of spatial variability, each designed to represent one possible seabed condition. Subsequently, piles were 'designed' using virtual CPT results typical of each site investigation (SI) strategy for each realization of the random field. Design used the ISO partial factor approach (LRFD) to fulfil in-place capacity requirements for a specified load distribution function. The probability of failure (p_f) of the pile designed using this method was then calculated (using

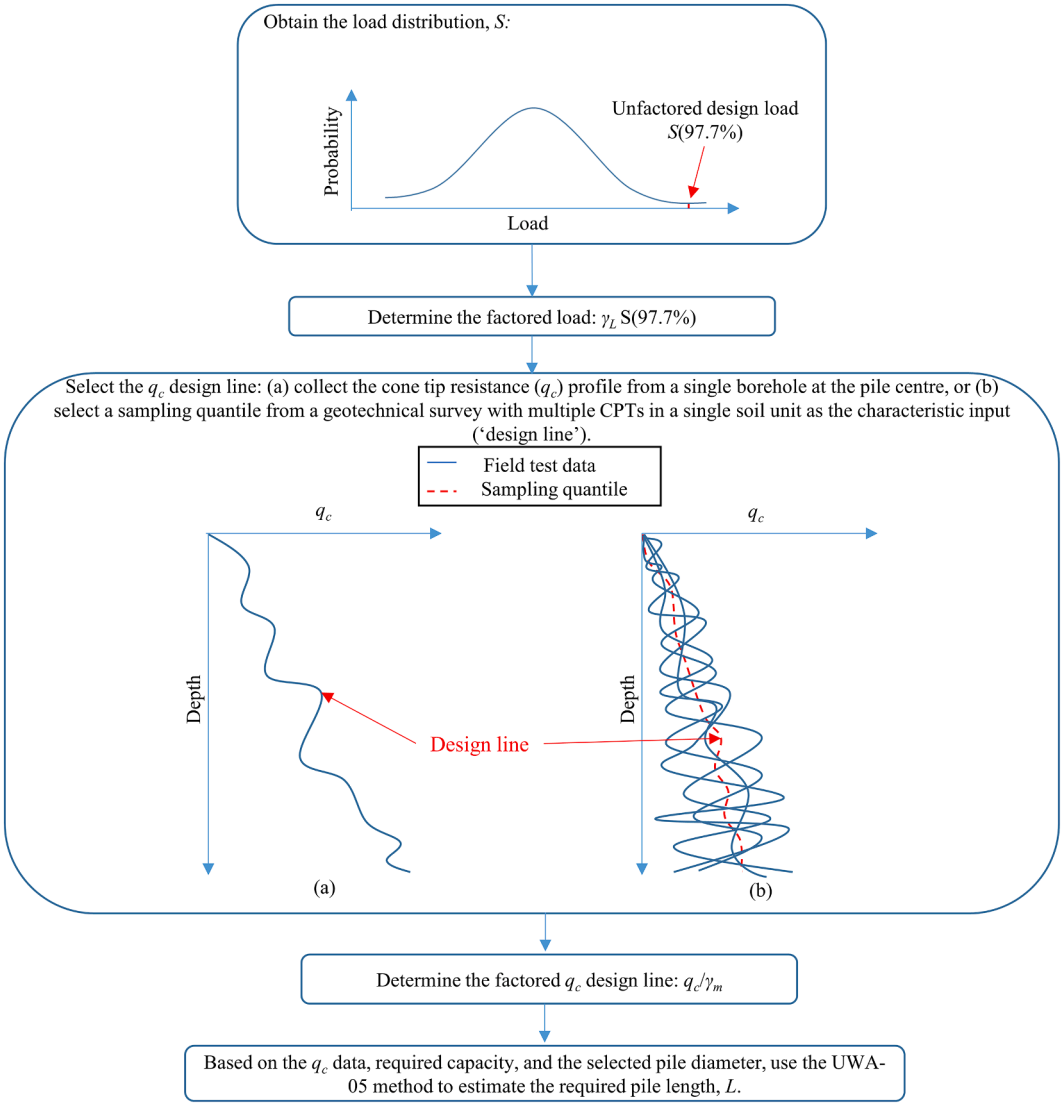

Fig. 2. Summary of pile design procedures.

knowledge of the full 3D seabed property field) and the results of multiple realizations were assembled to assess the suitability (or reliability) of the approach. This allowed recommendations to be made to modify standard deterministic partial factor design to incorporate explicitly the uncertainty in ground conditions.

2. Quantifying reliability of uplift capacity estimation in spatially variable soils

In this study, two design approaches for an open-end pile undergoing drained uplift loading are investigated. In the first case, the uplift capacity was calculated solely using a (virtual) single CPT tip resistance profile located at the center of the proposed pile. In the other approach, the uplift capacity of a pile positioned at an untested location was calculated using the aggregate data set from multiple (virtual) CPTs by selecting a characteristic design profile based on a given sample statistic (Phoon and Kulhawy, 1999; Uzielli et al., 2007; 2019;; Uzielli and Mayne, 2019). For each scenario of spatial variability, Monte Carlo simulations were performed for n realizations (the determination of n is discussed in Section 2.5) of the random field and the subsequent computation of the statistical distributions of pile uplift capacity and pile length, from which the reliability and probability of failure of the designed pile were evaluated.

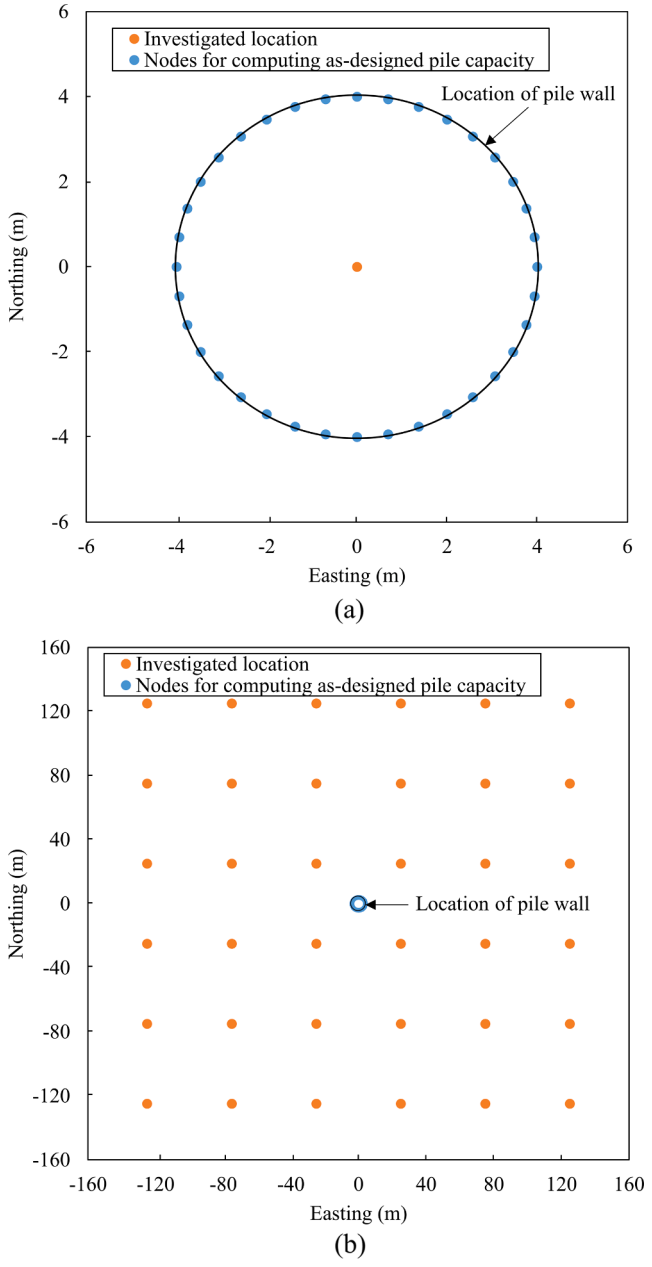

Fig. 3. Site geometries for: (a) the single-investigated location case; and (b) the multiple-investigated location case.

2.1. Pile design procedures

The pile sizing procedure was conducted using the ISO (2020) partial factor (or LRFD) approach as follows:

(1) Obtain the unfactored load that the foundation must resist. In this study, a lognormal annual uplift load (S) distribution with a mean of 12 MN and a coefficient of variation (i.e. the ratio between standard deviation and mean value) of 0.3 was used. This was selected to ensure that the majority of this distribution falls within the typical uplift load range for offshore wind turbines, i.e. 0 to 40 MN (Spagnoli et al., 2018). The deterministic design was assumed to have to withstand the P97.7 value of the load, i.e. S (97.7%), which is the load value corresponding to 97.7% (a typical design quantile, equivalent to the mean plus two standard deviations for a normal distribution) cumulative probability of the load distribution (20.65 MN in this case). The selected magnitude and distribution will affect the results of this exercise quantitatively, but not qualitatively (i.e. the general trends are expected to be unaffected).
(2) Multiply the unfactored load by a load factor, γ_L, to obtain the factored load, which the pile must withstand. The load factor $\gamma_L = 1.35$ corresponds to a 'live' environmental load (ISO, 2020). Consequently, the factored load for the example calculations is 27.88 MN.
(3) Calculate the required pile size for the given CPT design line so that the factored capacity ($R(q_c/\gamma_m)$, γ_m is the material factor) equals (or exceeds) the factored load (so $R(q_c/\gamma_m) \geq 27.88$ MN). Note that the soil property (q_c in this case) was divided by a material factor, $\gamma_m = 1.25$, before performing the calculation so that the output is the factored capacity.

The above can be summarized as:

$$R\left(\frac{q_c}{\gamma_m}\right) \geqslant \gamma_L S(97.7\%) \tag{1}$$

For the final set of calculations (i.e. step 3), the UWA-05 method (Lehane et al., 2005) was used to calculate the drained capacity of an open-ended pile based on the constant volume interface friction angle (δ_f), and the cone penetrometer resistance (q_c) data. The UWA-05 design equations (Lehane et al., 2005) are expressed as follows:

$$R\left(\frac{q_c}{\gamma_m}\right) = \pi D\left(\int \tau_f dz\right) tan\delta_f \tag{2a}$$

$$\tau_f = 0.0225\frac{q_c}{\gamma_m}\left\{1 - \left[1, \left(\frac{D}{1.5}\right)^{0.2}\left(\frac{D_i^2}{D}\right)\right]\right\}^{0.3}\left[max\left(\frac{h}{D}, 2\right)\right]^{-0.5} \tag{2b}$$

where τ_f is the local shaft friction; z is the depth below the seabed; D_i is

Table 1
Summary of cone tip resistance profile properties for random field generation.

Soil property	Symbol	Property value	Unit
Trend	μ_{qc}	See Eq. (3)	MPa
Mean relative density	D_r	80%	–
Coefficient of variation (COV)	COV(q_c)	0, 0.15, 0.3, 0.45	–
Horizontal scale of fluctuation	θ_h	0, 0.1D, 1D, 10D, 100D, ∞	m
Vertical scale of fluctuation	θ_v	1	m

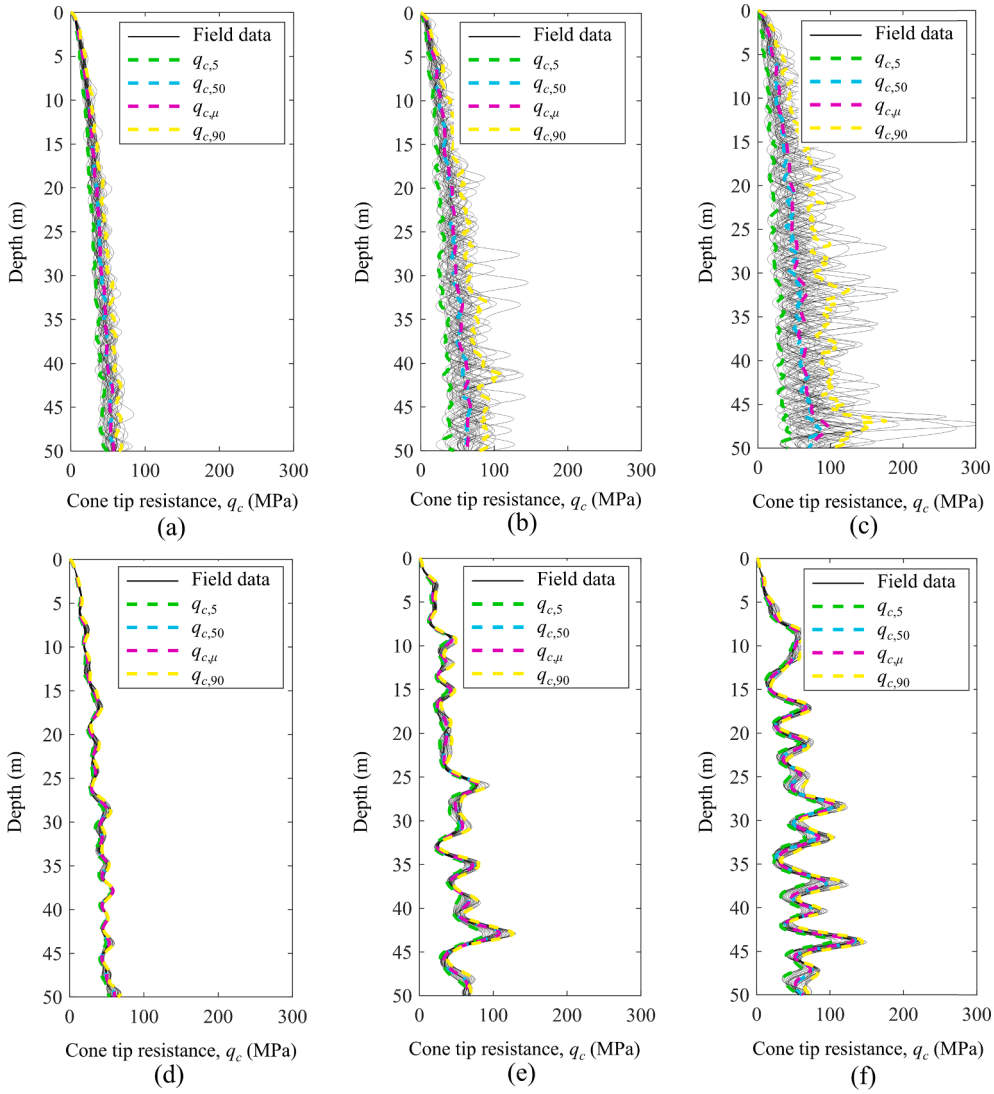

Fig. 4. Cone tip resistance profiles generated for: (a) COV(q_c) = 0.15, $\theta_h = 1D$; (b) COV(q_c) = 0.3, $\theta_h = 1D$; (c) COV(q_c) = 0.45, $\theta_h = 1D$; (d) COV(q_c) = 0.15, $\theta_h = 100D$; (e) COV(q_c) = 0.3, $\theta_h = 100D$; (f) COV(q_c) = 0.45, $\theta_h = 100D$ (50 m CPT spacing).

the inner diameter of the pile; and, h is the height above the pile tip.

Although model uncertainty is present in all axial pile capacity calculation methods including the UWA-05 method (Lehane et al., 2017), this uncertainty has not been included directly here in order to isolate uncertainty associated with selection of the characteristic (design) line.

Cone profile inputs are discussed below. A single deterministic value of $\delta_f = 29$ degrees was used in this study. This is because the interface friction angle is not expected to strongly correlate with cone tip resistance. The value of 29 degrees was selected based on recommendations for offshore steel pile design (Liu et al., 2019) based on a database of ring shear steel interface tests on sandy-silty soils which show a relatively low sensitivity of δ_f to fines contents, mineralogy, and normal stress level variations (though the correlation with q_c is believed to be unexplored).

In order to simplify the pile sizing process, the outer pile diameter, $D = 8$ m and the pile wall thickness $t = 100$ mm were fixed so that only the pile length, L, was varied to fulfil capacity requirements. The aforementioned value of the pile diameter was selected because a monopile with an outer diameter around 8 m has been installed in some European offshore wind facilities, e.g. Veja Mate offshore wind facilities (Negro et al., 2017). In addition, the ratio, $D/t = 80$ is commonly used in installed wind turbines (Arany et al., 2017). Although the above pile dimensions are typical of recent monopiles, the results of this study are presented normalized by pile diameter later so are equally applicable to smaller diameter anchor piles. As also demonstrated later the ratio of the pile diameter to the horizontal scale of fluctuation θ_h is more relevant to the problem investigated here than the pile diameter itself.

The pile sizing method is also summarized in Fig. 2.

2.2. Site geometry

This study investigates the reliability of two CPT-based pile design approaches (e.g. Fig. 2), corresponding to two distinct CPT sounding location geometries:

(1) In the single-investigated location geometry, a single CPT is 'conducted' at the center of the planned pile (Fig. 3a). The design line (and consequent pile length) was determined using this CPT data.
(2) In the multiple-investigated location approach, 36 CPTs are 'conducted' in a regular 6 by 6 grid with a 50 by 50 m spacing between grid points (Fig. 3b) with the anchor pile located at the center. Design relies on the data from the 36 CPTs to select the design q_c profile.

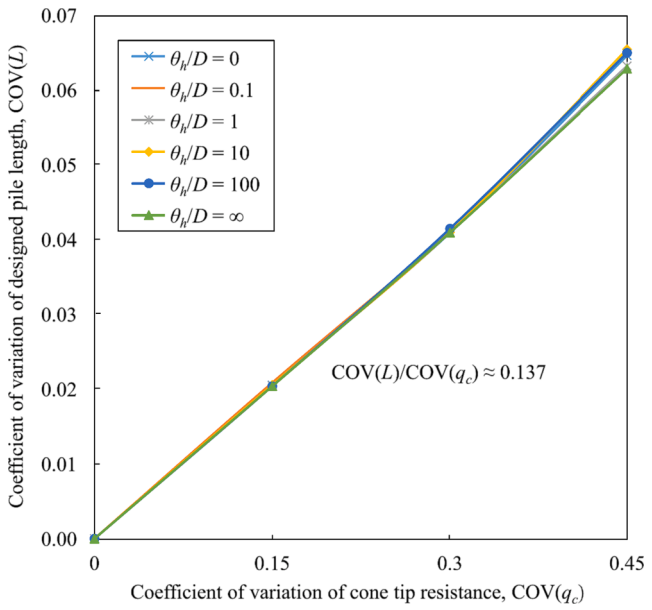

Fig. 5. Coefficient of variation of pile length designed with a single, centered CPT.

For both site geometries, the depth-wise sampling interval was 0.02 m (coinciding with a 2 cm/s cone penetration rate and minimum 1 Hz data logging specified in ISO (2014)).

2.3. As-designed capacity

For both site geometries, the as-designed pile capacity, $R(q_{ca})$, for each designed pile was calculated using the field data at pile wall location. This was done by 'revealing' 36 cone tip resistance profiles, q_{ca}, evenly distributed circumferentially around the pile wall at each depth (Fig. 3a and b). Thirty-six profiles were used because sensitivity analysis showed that increasing the mesh nodes from 36 to 360 only made a slight change (within 1%) to the computed $R(q_{ca})$.

Note that the recorded tip resistance of a cone penetrometer reflects an average across an influence zone around the cone tip. The influence zone usually extends from 2 CPT diameters in soft materials to up to 20 CPT diameters in stiff materials (e.g. 71.4 to 714 mm) (Ahmadi and Robertson, 2005; Rogers, 2006), which, for a typical CPT with a diameter of 35.7 mm is significantly smaller than the design pile diameter adopted herein. Hence, the CPT is assumed to give a point measurement of q_c in this study, although a significant spatial averaging effect may exist when the horizontal scale of fluctuation is smaller than the size of the cone influence zone (e.g. Zhang et al., 2020).

2.4. Modelling of spatial variability

The numerical work presented herein is limited to investigating a pile in a seabed with a single (sandy) soil unit which behaves in a drained manner during pile loading. This simplification has been made in order to isolate the already-complex statistics of the problem in order to examine design frameworks. Clearly, real seabed often have multiple soil layers or spatially trending changes in density or grading (e.g. Wang et al., 2018; 2019;; Montoya-Noguera et al., 2019; Zhao and Wang, 2020; Zhao et al., 2020) and the effect of these properties will worth studying in a second stage.

The vertical and horizontal spatial variability of q_c for a single silty sand layer can be expressed in terms of the superposition of a depth-wise trend (μ_{qc}) and a residual variation (reflecting the variability about the trend). The depth-wise trend of μ_{qc} is defined assuming that the average soil condition has a single relative density, D_r = 80%, with depth. The particular form of the trend is generated using the following equations (Lunne et al., 1997):

$$D_r = \frac{1}{2.61} ln\left[\frac{\mu_{qc}}{181\left(\sigma'_m\right)^{0.55}}\right] = \frac{1}{2.61} ln\left[\frac{\mu_{qc}}{181[(\gamma_{sat}-\gamma_w)z]^{0.55}}\right] \quad (3)$$

where σ'_m is the mean effective stress, γ_{sat} and γ_w (=10 kN/m^3) are the unit weight of saturated sand and water, respectively, and z is the depth below the seabed. For generating the depth-trend of q_c, a value of γ_{sat} = 22 kN/m^3 for silty sand with 80% of relative density was applied.

The spatial variability of q_c can be conveniently represented as a lognormal random field (e.g. Vanmarcke, 1984; Fenton and Griffiths, 2008; Cai et al., 2019) described by an autocorrelation function, a trend function (e.g. μ_{qc} in Eq. (3)), a coefficient of variation (COV(q_c)), and horizontal and vertical scales of fluctuation (θ_h and θ_v, respectively). The lognormal distribution prevents negative values and has been shown to be effective in simulating the spatial variability of cone tip resistance (Phoon and Kulhawy, 1999; Uzielli et al., 2007). The random fields were generated using the Karhunen-Loeve (KL) expansion method (Schwab and Todor, 2006). As the KL expansion needs to be truncated to a finite number of terms, a significant concern is that the simulated variance will be reduced. In order to control this reduction, the eigenvalues are sorted

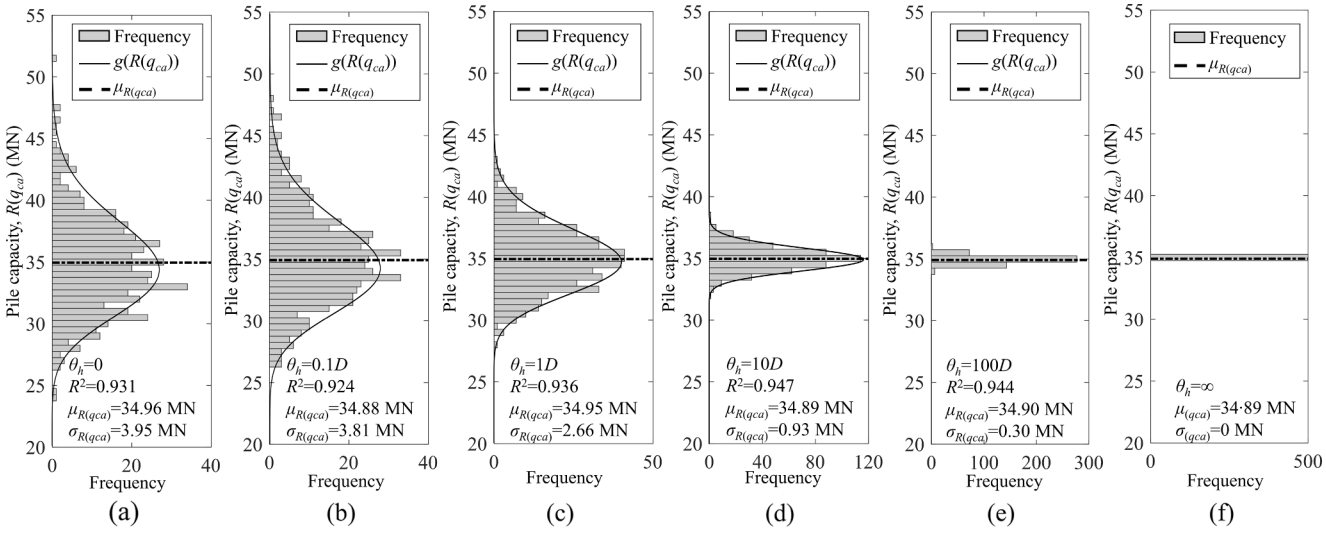

Fig. 6. Comparison of histogram and the probability density function of pile capacity, $R(q_{ca})$, with different θ_h when COV(q_c) = 0.45.

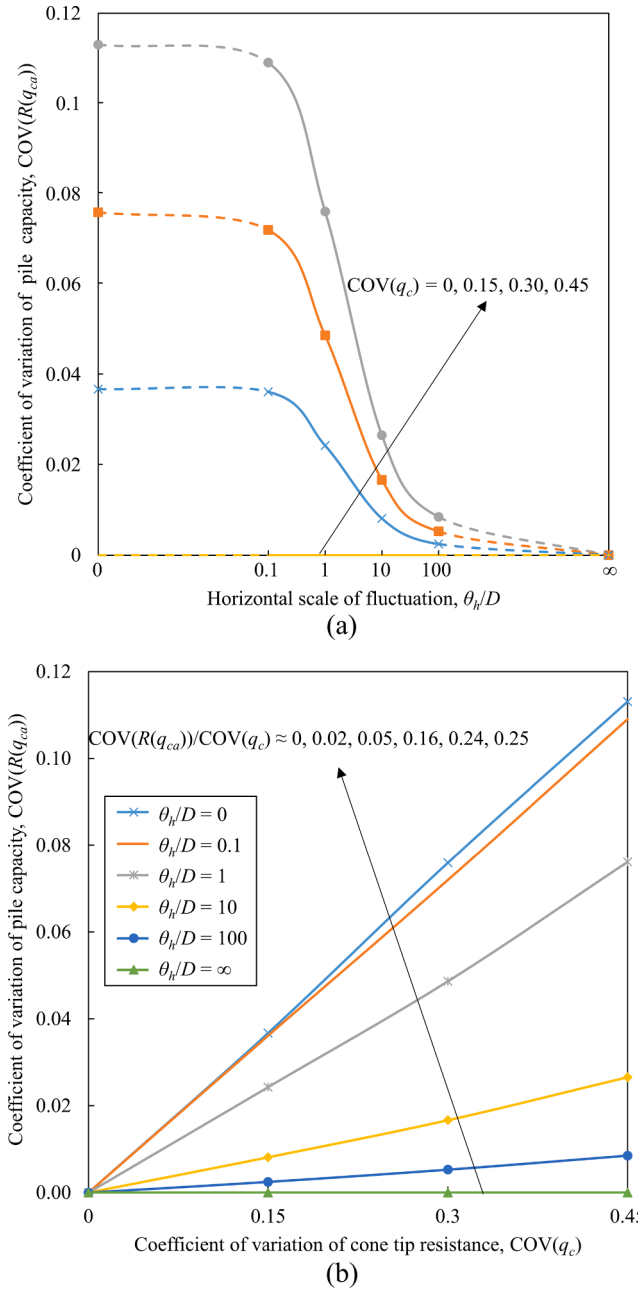

Fig. 7. Coefficient of pile capacity, COV($R(q_{ca})$), for different soil conditions: (a) variation of COV($R(q_{ca})$) with θ_h; (b) variation of COV($R(q_{ca})$) with COV(q_c).

in descending order and the number of terms decided when the last eigenvalue is at least ten thousand times smaller than the first eigenvalue. In addition, although the KL method only simulates Gaussian random fields, a lognormal random field can be easily obtained by substituting a Gaussian random field with a prescribed mean and standard deviation into the natural exponential function.

The scale of fluctuation is a measure of distance within which values of q_c can be considered strongly correlated. The autocorrelation function describes the correlation between values of residuals at locations j and k. An exponential autocorrelation function was chosen to characterize the spatial correlation (e.g. Zhu and Zhang, 2013; Li et al., 2015)

$$\rho_{jk} = exp\left[-2\left(\frac{\tau_{jk,h}}{\theta_h} + \frac{\tau_{jk,v}}{\theta_v}\right)\right] \quad (4)$$

where $\tau_{jk,h}$ and $\tau_{jk,v}$ are the distance between spatial points j and k in the horizontal and vertical directions, respectively. The other statistical properties of the q_c random field are presented in Table 1. Note that the typical range of vertical scale of fluctuation is between 0.1 and 2.2 m (Phoon and Kulhawy, 1999), which is usually much smaller than the pile length. Hence, the vertical scale of fluctuation was fixed at an intermediate value of 1 m in this study. A set of 24 site spatial variability scenarios for q_c were thus defined by combining values of the ratio of the horizontal scale of fluctuation of q_c to pile diameter (θ_h/D = 0, 0.1, 1, 10, 100, ∞) with values of the coefficient of variation of the lognormal distribution of cone resistance (COV(q_c) = 0, 0.15, 0.3, 0.45). For example, Fig. 4a–f show artificially generated q_c profiles (for site geometry shown in Fig. 3b) for combinations: (a) COV(q_c) = 0.15, θ_h = 1D; (b) COV(q_c) = 0.3, θ_h = 1D; (c) COV(q_c) = 0.45, θ_h = 1D; (d) COV(q_c) = 0.15, θ_h = 100D; (e) COV(q_c) = 0.3, θ_h = 100D; (f) COV(q_c) = 0.45, θ_h = 100D.

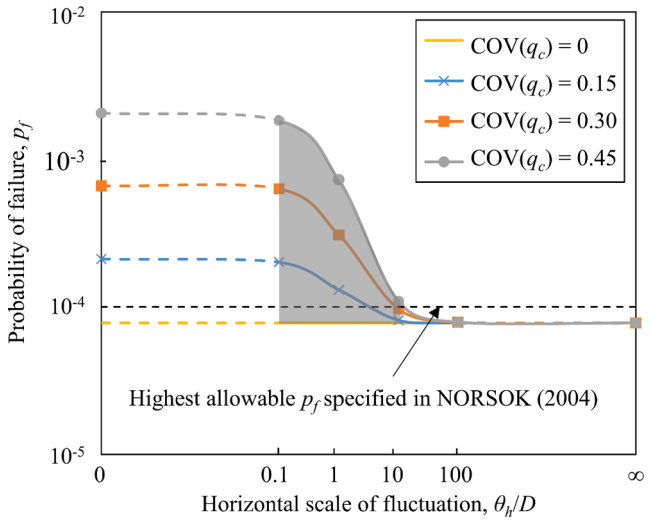

Fig. 8. Probability of failure of the designed pile evaluated from $g(R(q_{ca}))$ and $f(S)$.

2.5. Monte Carlo simulation

For each spatial variability scenario as described above, 500 realizations of the q_c random field were generated. For each realization, the pile length was calculated to fulfil the partial factor requirements for uplift capacity as discussed above, and the as-designed pile capacity, $R(q_{ca})$, was calculated for that pile length. The results of all realizations was collated, and the sample statistics of calculated pile length and of the as-designed pile capacity were calculated.

The number of realizations for the Monte Carlo analyses was selected theoretically and checked empirically. The error, *err*, with confidence (1-α) in the estimate of the mean and COV of a random field from the n realizations can be calculated by (Fenton and Griffiths, 2008):

$$err \approx \frac{z_{\alpha/2}\mathrm{COV}(q_c)}{\sqrt{n}} \quad (5)$$

where $z_{\alpha/2}$ is the value of the standard normal variate with a cumulative probability level (1- α/2). When the number of simulations is 500, the maximum error *err* is less than 0.1 times the COV(q_c) (3.95% for COV of 0.45) with a confidence of 95%. An empirical check showed that when n = 500, the variation ranges between 2.5% and 97.5% quantiles of the mean values of L (μ_L) and of $R(q_{ca})$ ($\mu_{R(qca)}$), and the coefficients of variation of L (COV(L)) and of $R(q_{ca})$ (COV($R(q_{ca})$)) are −0.6%~0.7%, −0.1%~0.1%, −3.3%~3.8%, and −2.8%~3.1% compared to the median, respectively. These ranges of variation are smaller than the maximum error, *err* (=3.95%), calculated by Eq. (5).

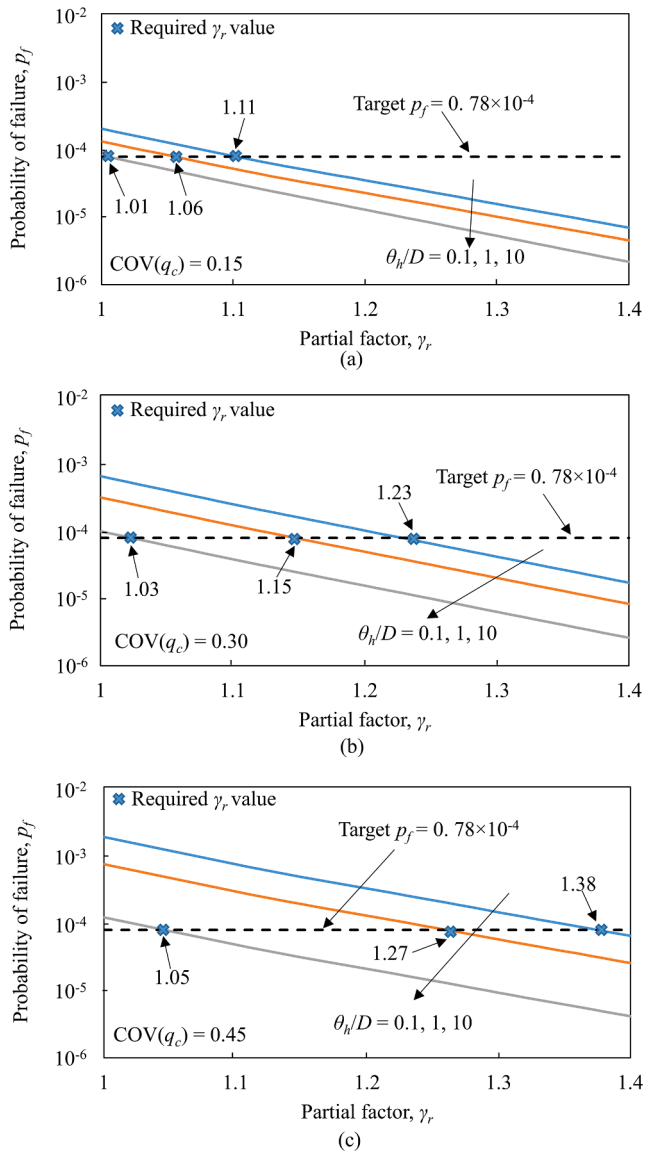

Fig. 9. Probability of failure computed from $g(R(q_{ca}))$ after using different γ_r values for different combinations of COV(q_c) and θ_h/D: (a) COV(q_c) = 0.15; (b) COV(q_c) = 0.3; and (c) COV(q_c) = 0.45.

2.6. Probability of failure calculation

Once the annual probability distribution of the uplift loading, $f(S)$, and the as-designed pile capacity, $g(R(q_{ca}))$, are obtained, the annual probability of failure, p_f, for the designed pile can be evaluated as:

$$p_f = \iint_{R(q_{ca})\leqslant S} f(S)g(R(q_{ca}))dR(q_{ca})dS \tag{6}$$

In this study, $g(R(q_{ca}))$ was estimated by fitting the histogram of Monte Carlo-calculated $R(q_{ca})$ values with a suitable distribution (discussed in Section 3). The uplift loading distribution ($f(S)$) was assumed to be lognormal with a mean of 12 MN and a COV of 0.3 (as described earlier).

3. Results of numerical analyses

3.1. Single-CPT case

3.1.1. Calculated pile length statistics

For all sets of soil conditions, the mean calculated pile length, μ_L, for the single-CPT case and standard ISO partial factors is 23.2 m, which is equivalent to the calculated pile length from the deterministic, mean-strength case (i.e., when COV(q_c) = 0). This result is to be expected, because the mean of the pile lengths will depend on the deterministic mean of the soil property.

Fig. 5 presents the relationship between the resulting COV of the calculated pile length (COV(L)) and the input COV of the soil (COV(q_c)). The relationship is approximately linear, i.e., COV(L)/COV(q_c) ≈ 0.137. The fact that the gradient is much smaller than unity indicates that the variability of the pile length is much smaller than the variability of the soil properties (because of the non-linearity of the pile length to capacity relationship), but there is still a significant variability of the calculated pile length (e.g. the variation ranges for cases with COV(q_c) of 0.15, 0.3, and 0.45 are around 21 ~ 25 m, 20 ~ 27 m, and 18 ~ 29 m, respectively). Furthermore, the relationship is essentially independent of the horizontal scale of fluctuation. This follows from the fact that because only one CPT is used in this design approach there is no comparison data in the horizontal direction to reveal the horizontal correlation of the soil properties and therefore this is not considered in the estimation of pile length, L.

3.1.2. Statistics of pile capacity

It is of interest to assess the suitability of this design approach (i.e. of assuming no horizontal variability and designing based only on the data from a single centered CPT). This is pursued by comparing the unfactored design capacity, $R(q_c)$ (= 34.89 MN), and the calculated as-designed capacity, $R(q_{ca})$, of the pile considering the entire random field around the pile perimeter, and calculating the probability of failure of the designed pile based on the distribution of $R(q_{ca})$ and the specified distribution of the design load.

The probability distribution of $R(q_{ca})$ was evaluated by fitting the Monte Carlo-produced histogram of $R(q_{ca})$ with a lognormal density function. For example, the statistics of $R(q_{ca})$ for the cases where COV (q_c) = 0.45 are illustrated in Fig. 6 by showing the histograms of $R(q_{ca})$ for designed piles for different θ_h/D ratios. Each histogram was fitted by a lognormal probability density function, $g(R(q_{ca}))$, with a mean, $\mu_{R(qca)}$, and a standard deviation, $\sigma_{R(qca)}$ (with values provided in Fig. 6). A lognormal distribution appears to adequately represent the capacity distribution as the coefficient of determination, R^2, for these fittings are all larger than 0.90 (as illustrated in Fig. 6).

For all sets of soil conditions, the mean capacity $\mu_{R(qca)}$ (e.g. Fig. 6) is close to the required unfactored design capacity (i.e., 34.89 MN) from the deterministic, mean-strength case (i.e., when COV(q_c) = 0), because, as discussed above, μ_L is not influenced by the spatial variability of the soil properties. However, the CPT-measured q_c becomes less representative of the spatially averaged q_{ca} around the pile wall as the horizontal scale of fluctuation decreases, resulting in a wider distribution of $R(q_{ca})$ (e.g. Fig. 6). This variation of $g(R(q_{ca}))$ is quantified as the COV of the capacity (COV($R(q_{ca})$)) (calculated from the fitted lognormal distribution) and is plotted against the horizontal scale of fluctuation for different COV(q_c) conditions in Fig. 7a (where the (highest) grey line represents the conditions shown in Fig. 6). COV($R(q_{ca})$) increases linearly with the overall variability of the soil properties (i.e. as COV(q_c) increases) as shown on Fig. 7b and reduces non-linearly with the horizontal scale of fluctuation (see Fig. 7a).

The form of the relationships shown in Fig. 7(a) can be understood by considering comparatively the cases with $\theta_h/D \to \infty$ and $\theta_h/D \to 0$. When the horizontal spatial correlation scale is very large ($\theta_h/D \to \infty$), at any given depth, the soil in the whole zone of influence of the pile (including the CPT location) has the same q_c value for any given realization. Consequently, the CPT accurately reflects the spatially averaged q_c in the influence zone of the pile and so COV($R(q_{ca})$) → 0. In contrast, when the horizontal spatial correlation scale is very small (i.e. as $\theta_h/D \to 0$), spatial averaging around the pile results in the pile capacity reflecting the mean q_c value with no variability in $R(q_{ca})$ (i.e. COV($R(q_{ca})$) = 0) for a given pile length. However, the pile length for each design realization

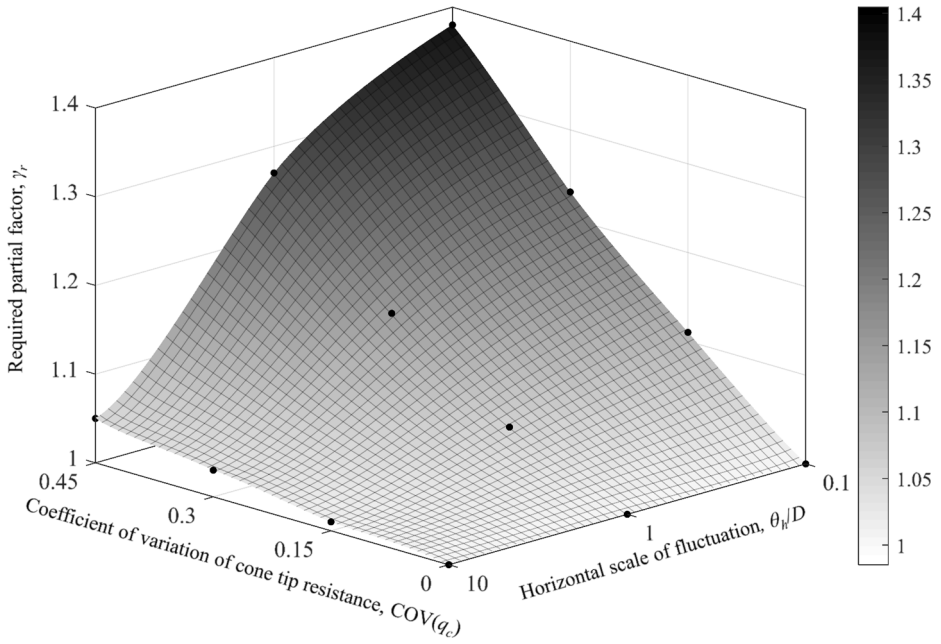

Fig. 10. Required partial factor to achieve target pile reliability for the single-CPT design approach.

is selected based on the CPT data (which represents the strength at a point location and has a COV equal to that of the general COV population) and so there is an increased COV of the designed pile capacity.

A larger COV($R(q_{ca})$) indicates a larger variation of the capacity of the designed piles among different realizations generated from the same combination of soil variability parameters. This variation is significant when the normalized horizontal scale of fluctuation $\theta_h/D < 10$ for the conditions investigated herein. A typical range of horizontal scales of fluctuation of q_c in natural seabed of 3 to 80 m (Phoon and Kulhawy, 1999) implies a range of $0.3 < \theta_h/D < 8$ for a 10 m diameter (mono) pile and $1.5 < \theta_h/D < 40$ for a 2 m diameter (anchor) pile and so this effect may be significant. This significance is quantified in Section 3.1.3 by examining how the design reliability (annual probability of failure) of a pile is affected by this phenomenon for the example load distribution.

3.1.3. Reliability of the designed piles

Based on Eq. (6), the expected p_f of the designed pile evaluated from the unfactored design capacity (34.89 MN) and the probability density function of the specified load, $f(S)$, was 0.79×10^{-4}, which is close to the highest allowable annual probability of failure (10^{-4}) specified in the Norwegian standard (Norsok, 2004) for the reliability of manned installations. However, the p_f evaluated using $R(q_{ca})$ and $f(S)$ varies with soil conditions, because of the variation of 'designed' pile capacity distribution $g(R(q_{ca}))$ as discussed earlier. For example, Fig. 8 presents the relationship between p_f of the designed piles and θ_h/D for COV(q_c) = 0, 0.15, 0.3, and 0.45. Decreasing COV(q_c) or increasing θ_h results in p_f approaching the expected value ($=0.79 \times 10^{-4}$). However, for cases where θ_h is smaller than approximately 10D, the probability of failure is higher than targeted, i.e., the designed piles have a lower reliability than expected. This indicates that for a typical range of θ_h from 3 to 80 m and a pile diameter of 8 m (so $\theta_h/D = 0.375$ to 10; shown shaded in Fig. 8), the calculated p_f of a pile considering horizontal variability of q_c is larger than the expected value. Consequently, simply using the q_c profile from a single CPT to design a large pile appears to result in unconservative design even when code-recommended resistance and material partial factors are used.

3.1.4. Calibration of partial factor for q_c profile

One way of avoiding the overestimation in reliability is to apply an additional partial factor (γ_r) to the q_c profile (i.e. to scale down the CPT resistance curve) to allow for the fact that the spatially averaged q_c value around the pile may be lower than measured because of horizontal spatial variability. Use of this additional partial factor would then result in the following overall design requirement:

$$R\left(\frac{q_c}{\gamma_m \gamma_r}\right) \geqslant \gamma_L S(97{\cdot}7\%) \tag{7}$$

In order to select a partial factor γ_r to achieve the expected reliability, the probability of failure computed from $g(R(q_{ca}))$ after using different γ_r values is plotted in Fig. 9 for different combinations of COV(q_c) and θ_h/D. From these relationships the recommended partial factors to achieve $p_f = 0.78 \times 10^{-4}$ were selected with the values summarized in Fig. 9 and shown on Fig. 10. As expected, the required partial factors increase with reducing horizontal θ_h/D and increasing COV(q_c). For example, as the COV(q_c) varies from 0.15 to 0.45, the calibrated partial factor for the case with $\theta_h = 8$ m and D = 8 m (i.e. $\theta_h/D = 1$) varies from 1.06 to 1.27. Therefore, even if the pile is constructed at a tested location, it may be necessary to account for the spatial variability of soil properties. The approach used here allows the conditions when such a scaling is required to be identified, although more work is required to use this framework to generalize the findings to a wider range of conditions.

3.2. Multiple-CPT case

When a pile is designed using data from multiple locations, the characteristic profile (the design line) may be established by considering a specific sample statistic, depending on the limit state being examined and the foundation type (Marques et al., 2011; Pohl, 2011; Lacasse et al., 2013). Typical sample statistics adopted include the 5% sample quantile ($q_{c,05}$), sample mean minus half sample standard deviation ($q_{c,(\mu\text{-}0.5\sigma)}$), sample mean ($q_{c,\mu}$), and sample median ($q_{c,50}$) (EN, 2004; 2007;; Marques et al., 2011). This section quantifies the reliability of piles designed using different sample statistic quantiles and discusses the optimal sample statistic for the design case examined here.

3.2.1. Calculated pile length statistics

Fig. 11 shows how the mean and COV of the 'designed' pile length vary with the horizontal scale of fluctuation for different COV(q_c) conditions using different sample statistics to select the characteristic design line. Although the 90% quantile ($q_{c,90}$) is rarely used in pile design, this

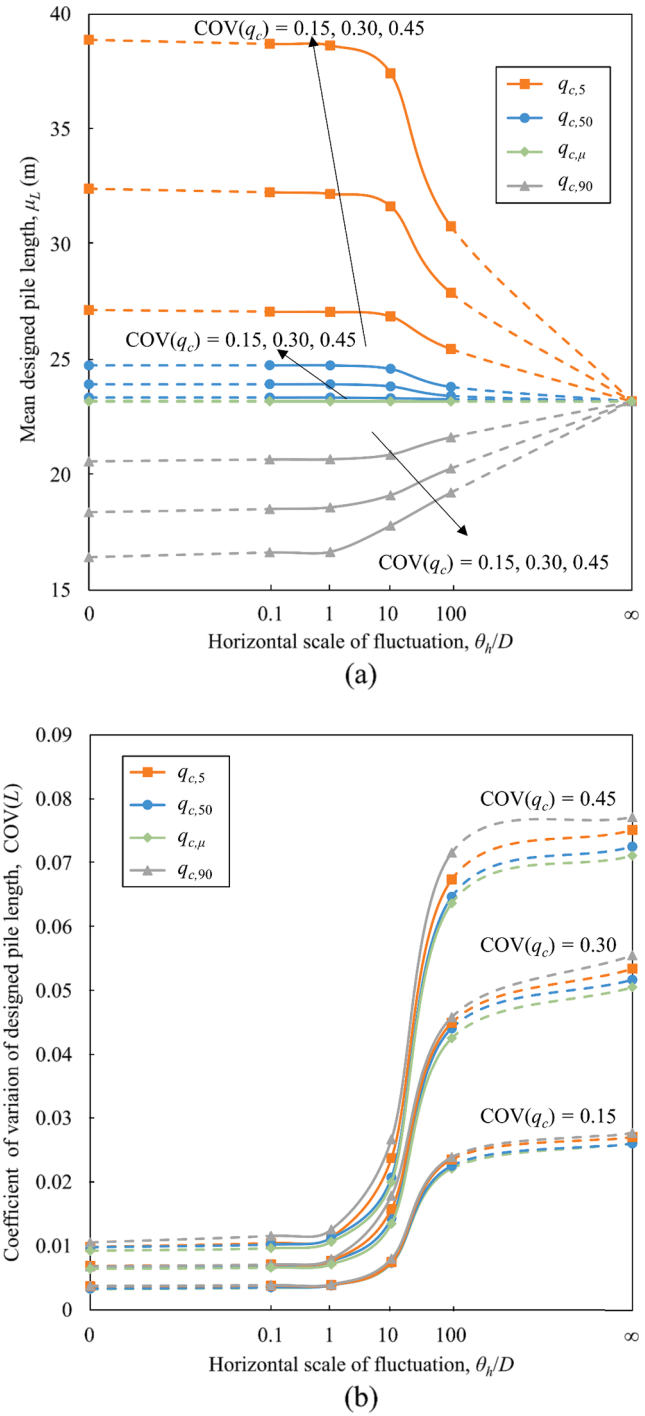

Fig. 11. Variation of: (a) μ_L; and (b) COV(L) with θ_h/D.

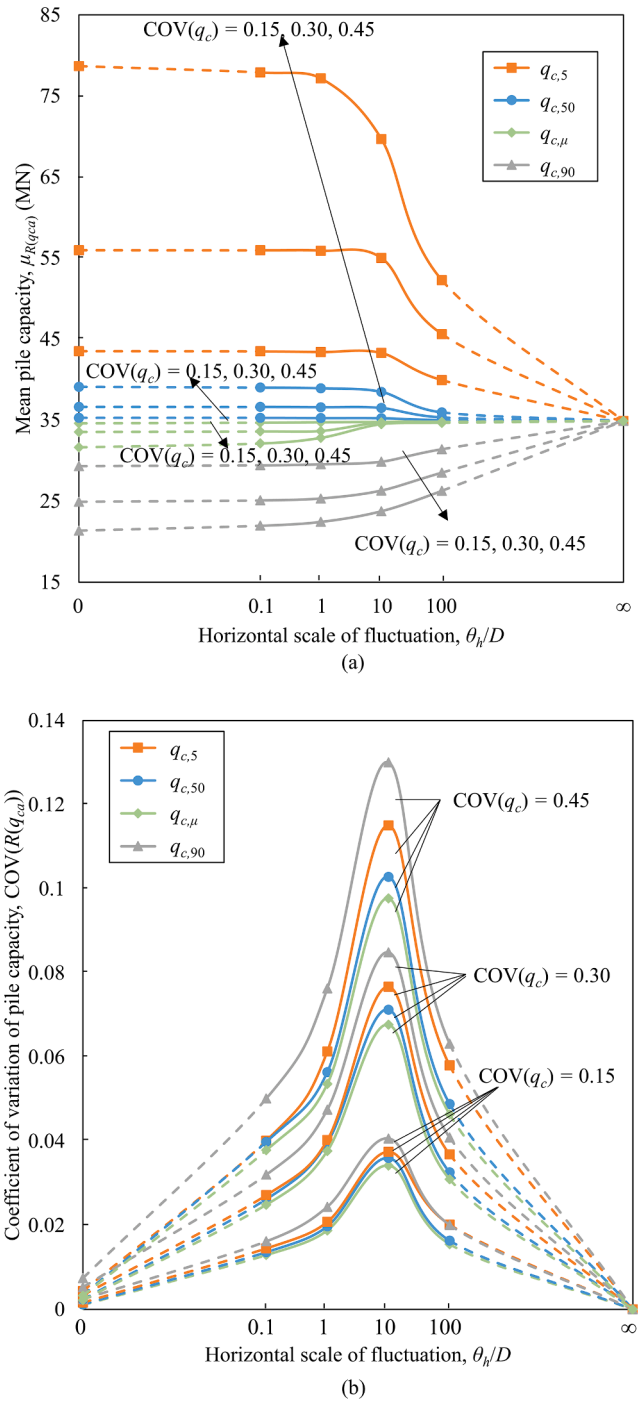

Fig. 12. Variation of (a) $\mu_{R(qca)}$ and (b) COV($R(q_{ca})$) with θ_h/D.

is included here for the purpose of demonstration. Obviously, the designed pile length becomes more conservative (i.e. has a higher mean length, μ_L, as shown in Fig. 11a) as the sample quantile decreases (e.g., from 90% to 5%). However, the difference between μ_L designed by $q_{c,05}$, $q_{c,50}$, $q_{c,\mu}$, and $q_{c,90}$ becomes smaller and closer to 23.2 m (the designed pile length for the case where COV(q_c) = 0) as COV(q_c) decreases or as θ_h increases. This is because the range of values in the q_c profiles at each depth for any given realization decreases with increasing θ_h (because the site becomes horizontally uniform) or decreasing COV(q_c) (because the overall variability reduces). This is shown in Fig. 4, where $q_{c,05}$, $q_{c,50}$, $q_{c,\mu}$, and $q_{c,90}$ converge for the θ_h/D = 100 condition (Fig. 4d–f). Consequently, this results in smaller differences between the mean pile lengths designed using the four statistical values $q_{c,05}$, $q_{c,50}$, $q_{c,\mu}$, and $q_{c,90}$ as θ_h/D $\rightarrow\infty$.

The variability of the designed pile length (COV(L)) increases non-linearly with increasing COV(q_c) and θ_h as shown in Fig. 11b. Essentially, a larger COV of the designed pile length (COV(L)) is a result of a larger variation of selected design lines between different realizations for any soil condition. As mentioned above, when θ_h is very large each 'site' (realization) is effectively horizontally uniform and so the COV of the design values at any depth is equal to the COV of the point statistics. In addition, a larger COV(q_c) results in a wider distribution of the seabed strengths, which leads to a more significant variation of the sample quartiles between different realizations (e.g. Fig. 4).

Both μ_L and the COV(L) are independent of θ_h when $\theta_h/D < 1$. This is

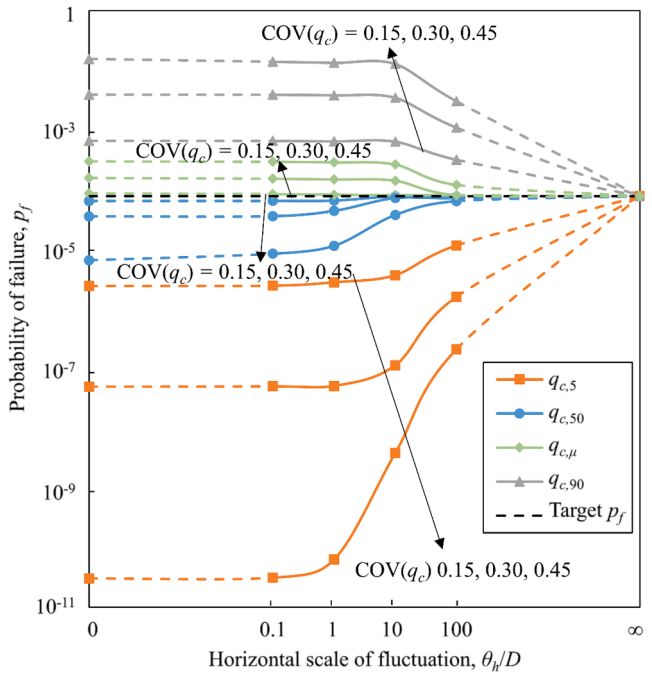

Fig. 13. Influence of variability of q_c on estimated p_f evaluated from $g(R(q_{ca}))$ and $f(S)$.

attributed to the relative magnitude of θ_h and the horizontal CPT spacing. When θ_h is much smaller than the CPT spacing, the 36 q_c profiles are independent of each other and their values are no longer influenced by the exact value of θ_h.

3.2.2. Statistics of pile capacities

The capacity of the piles $R(q_{ca})$ 'designed' using each q_c quantile (e.g. $q_{c,05}$, $q_{c,50}$, $q_{c,\mu}$, and $q_{c,90}$) are shown in Fig. 12. The mean capacity, $\mu_{R(qca)}$, shows a variation pattern similar to that of μ_L, while the variation of the COV of $R(q_{ca})$ is not monotonic with regards to θ_h. For all cases in this study, the COV($R(q_{ca})$) always reaches a peak value when $\theta_h \approx 10D$ (or $\theta_h \approx$ CPT spacing, i.e. 50 m) and reduces with increasing or decreasing θ_h (Fig. 12b). This is because when the horizontal scale of fluctuation is very large (i.e. $\theta_h/D \rightarrow \infty$), the values of $q_{c,05}$, $q_{c,50}$, $q_{c,\mu}$, and $q_{c,90}$ approach the (same) q_c profile everywhere around the pile. Consequently, the pile capacity for each realization should be close to the required design resistance (and so COV($R(q_{ca})$) $\rightarrow$ 0). In contrast, when the horizontal scale of fluctuation is small (i.e. θ_h is smaller than the CPT spacing), the variations in q_c are averaged around the perimeter of the large diameter pile and so with decreasing horizontal scale of fluctuation, the averaged q_c falls closer to the mean q_c of the site. Hence, the variation of the pile capacity becomes smaller. Finally, as expected, COV($R(q_{ca})$) increases approximately linearly with COV(q_c) for any given value of θ_h/D and strength quantile.

3.2.3. Reliability of the designed piles

Once the $\mu_{R(qca)}$ and COV($R(q_{ca})$) are obtained, the probability of failure considering soil variability around the pile can be evaluated using Eq. (6). As shown in Fig. 13, only when θ_h is infinite does the estimated p_f matches the target probability of failure perfectly. When the pile is designed using $q_{c,05}$ or $q_{c,50}$, p_f decreases as the scale of fluctuation θ_h reduces (i.e. the pile becomes increasingly over-designed). In contrast, p_f increases (i.e. the pile becomes 'unsafe') when piles are designed using a characteristic line based on $q_{c,\mu}$ or $q_{c,90}$. This indicates that when $\theta_{h/B} \leq$ 10, it is overly cautious to design using a characteristic line based on $q_{c,05}$ and unsafe to design based on $q_{c,\mu}$ or $q_{c,90}$. For the lognormal soil distribution used here, using a characteristic line based on the median of the q_c population (i.e. $q_{c,50}$) appears to yield an acceptable result as the probability of failure remains appropriately positioned on the 'safe' side of the target value even for small θ_h/D values.

4. Summary and conclusions

This paper explores the accuracy of CPT-based design methods for large diameter piles in spatially variable soil by quantifying the resulting annual probability of failure for piles in axial tension sized using partial factor (ISO LRFD) approaches using two different form of CPT inputs.

The following conclusions are drawn:

(1) When a pile is designed solely using a single CPT at its center, the accuracy of the pile capacity estimation is highly dependent on the ratio between the horizontal scale of fluctuation and the diameter of the pile, and the COV of the soil property. When the scale of fluctuation is large compared to the pile diameter, using only a single CPT to quantify capacity will result in achieving targeted reliabilities. However, when the scale of fluctuation is small compared to the pile diameter, using only a single CPT to quantify capacity may result in lower than code-tolerated foundation reliabilities. This can be corrected by applying a suitable partial factor (γ_r) to scale down the CPT resistance profile to account for potential spatial variability. An approach to calculate the required value of γ_r depending on the spatial variability (i.e. θ_h/D) and overall COV of the seabed properties is proposed, with values evaluated for one combination of site and pile conditions. Additional work is required to investigate the specific values of partial factors to encompass a broader range of load distributions, soil conditions, and target probabilities of failure, but the framework presented here is expected to be equally relevant.

(2) When selecting a design line using a fixed sample statistic of a large population of geotechnical data in a single soil unit to design a large diameter pile subject to axial tension, the reliability of the pile capacity estimation decreases as the coefficient of variation of cone resistance (i.e. COV(q_c)) increases as expected, but also appears to be most unreliable when the horizontal scale of fluctuation is approximately ten times the pile diameter (i.e. $\theta_h/D \approx 10$) or the minimum CPT spacing (i.e. 50 m in the example shown). In addition, the reliability of this design method is significantly influenced by the selected sample statistic with the use of low quartiles (e.g. $q_{c,05}$) leading to excessively high reliability (i.e. low values of p_f). In this study, the optimal sample statistic for design is around $q_{c,50}$, for a pile which is long compared to the vertical scale of fluctuation for the lognormal soil property distribution used.

Finally, some aspects of system response were ignored in order to isolate the difference in design outcomes for different CPT-based design approaches. For example, pile design reliability will also be influenced by other factors such as the uncertainty of the capacity calculation model and measurement uncertainty. In addition, a seabed condition with only a single soil layer was considered and the paper focuses on axial tensile capacity for simplicity. However, it is believed that the design framework explored has general applicability for broader seabed conditions, pile loadings and pile geometry combinations.

Declaration of Competing Interest

The authors declare that they have no known competing financial interests or personal relationships that could have appeared to influence the work reported in this paper.

Acknowledgements

The authors would like to acknowledge the funding support provided by the Australian Renewable Energy Agency under project ARENA-

2015-RND086. The work presented in this paper is part of the research activities undertaken by the Centre for Offshore Foundation Systems within the Oceans Graduate School at the University of Western Australia. The second author holds the Fugro Chair in Geotechnics whose support is gratefully acknowledged.

References

Ahmadi, M., Robertson, P., 2005. Thin-layer effects on the CPT qc measurement. Can. Geotech. J. 42 (5), 1302–1317. https://doi.org/10.1139/t05-036.

API, 2014. Recommended practiec for planning, designing, and constructing fixed offshore plateforms – working stress design, 22nd ed". American Petroleum Institute, Washington (DC).

Arany, L., Bhattacharya, S., Macdonald, J., Hogan, S., 2017. Design of monopiles for offshore wind turbines in 10 steps. Soil Dyn. Earthq. Eng. 92, 126–152. https://doi.org/10.1016/j.soildyn.2016.09.024.

Byrne, B.W., Mcadam, R., Burd, H.J., Houlsby, G.T,, Martin, C.M., Zdravkovic, L., Taborda, D.M.G., Potts, D.M., Jardine, R.J., Sideri, M., Schroeder, F.C., Gavin, K., Doherty, P., Igoe, D., Muir Wood, A., Kallehave, D., Skov Gretlund, J., 2015. New design methods for large diameter piles under lateral loading for offshore wind applications. In: 3rd International Symposium on Frontiers in Offshore Geotechnics – ISFOG, Oslo, Norway; 2015. pp. 705-710. https://doi.org/10.1201/b18442-96.

Cai, Y., Li, J., Li, X., Li, D., Zhang, L., 2019. Estimating soil resistance at unsampled locations based on limited CPT data. Bull. Eng. Geol. Environ. 78 (5), 3637–3648. https://doi.org/10.1007/s10064-018-1318-2.

Dechiron, C., Coste, F., Erbrich, C., Heerkes, M., Lange, F., Frankenmolen, S., Van Haaften, E., 2020. Prelude FLNG Driven Anchor Piles in Australian Carbonate Soils: Free-Fall Risk Management by Design. In: Proceedings of Offshore Technology Conference, Houston, Texas, USA; May 2020. https://doi.org/10.4043/30492-MS.

EN, 2004. Eurocode 7: Geotechnical design - Part 1: General rules, 1997-1. European Committee for Standardization, Brussels.

EN, 2007. Eurocode 7: Geotechnical design - Part 2: Ground investigation and testing, 1997-2. European Committee for Standardization, Brussels.

Erbrich, C., Lam, S.Y., Zhu, H., Derache, A., Sato, A., Al-Showaiter, A., 2017. Geotechnical design of anchor piles for Ichthys CPF and FPSO. In: Proceedings of Offshore Site Investigation Geotechnics 8th International Conference, Society for Underwater Technology; 2017. 1186(1197): pp. 1186-1197. https://doi.org/10.3723/OSIG17.1186/.

Fenton, G.A., Griffiths, D.V., 2008. Risk assessment in geotechnical engineering. Wiley, New York.

ISO, 2014. Petroleum and natural gas industries – Specific requirements for offshore structures – Part 8: Marine soil investigations, ISO 19901-8. International Standards Organization.

ISO, 2020. Petroleum and natural gas industries-fixed steel offshore structures, ISO 19902. International Standards Organization.

Kallehave, D., Byrne, B.W., LeBlanc Thilsted, C., Mikkelsen, K.K., 2015. Optimization of monopiles for offshore wind turbines. Philos. Trans. Roy. Soc. A: Math. Phys. Eng. Sci. 373 (2035), 20140100. https://doi.org/10.1098/rsta.2014.0100.

Klinkvort, R.T., 2012. Centrifuge modelling of drained lateral pile - soil response: Application for offshore wind turbine support structures. Ph.D. Thesis, Technical University of Denmark.

Lacasse, S., Nadim, F., Knudsen, S., Eidsvig, U.K., Liu, Z.Q., Yetginer, G., Guttormsen, T. R., 2013. Reliability of axial pile capacity calculation methods. In: GéoMontréal 2013, the 66th Canadian Geotechnical Conference, Montreal, Quebec, Canada; Sept.-Oct. 2013.

Lehane, B., Lim, J.K., Carotenuto, P., Nadim, F., Lacasse, S., Jardine, R.; van Dijk, B., 2017. Characteristics of Unified Databases for Driven Piles. In: Proceedings of the 8th Offshore Site Investigation and Geotechnics International Conference, Society for Underwater Technology; 2017. pp. 162-194. https://doi.org/10.3723/OSIG17.162.

Lehane, B., Schneider, J., Xu, X., 2005. The UWA-05 method for prediction of axial capacity of driven piles in sand. In: Proceedings of the International Symposium on Frontiers in Offshore Geotechnics (eds M. J. Cassidy and S. Gourvenec), The Netherlands: CRC Press, Balkema; 2005. pp. 683-689. https://doi.org/683-689. 10.1201/NOE0415390637.ch76.

Li, J., Cai, Y., Li, X., Zhang, L., 2019. Simulating realistic geological stratigraphy using direction-dependent coupled Markov chain model. Comput. Geotech. 115, 103147 https://doi.org/10.1016/j.compgeo.2019.103147.

Li, J., Tian, Y., Cassidy, M., 2015. Failure mechanism and bearing capacity of footings buried at various depths in spatially random soil. J. Geotech. Geoenviron. Eng. 141 (2), 04014099. https://doi.org/10.1061/(ASCE)GT.1943-5606.0001219.

Liu, T.F., Quinteros, V.S., Jardine, R.J., Carraro, J.A.H., Robinson, J., 2019. A Unified database of ring shear steel-interface tests on sandy-silty soils. In: Proceedings of XVII European Conf. Soil Mech. and Geotechnical Engg., Reykjavik, Iceland; 2019. https://doi.org/10.32075/17ECSMGE-2019-0268.

Lunne, T., Robertson, P.K., Powell, J.J.M., 1997. Cone Penetration Testing in Geotechnical Practice. CRC Press.

Marques, S.H., Gomes, A.T., Henriques, A.A., 2011. Reliability assessment of Eurocode 7 retaining structures design methodology. In: Proceedings of the 3rd Int. Symp. on Geotechnical Safety and Risk (ed. N. Vogt), Karlsruhe, Germany: Bundesanstalt für Wasserbau; 2011. pp. 455-462.

Montoya-Noguera, S., Zhao, T., Hu, Y., Wang, Y., Phoon, K.K., 2019. Simulation of non-stationary non-Gaussian random fields from sparse measurements using Bayesian compressive sampling and Karhunen-Loève expansion. Struct. Saf. 79, 66–79. https://doi.org/10.1016/j.strusafe.2019.03.006.

Negro, V., López-Gutiérrez, J., Esteban, M., Alberdi, P., Imaz, M., Serraclara, J., 2017. Monopiles in offshore wind: preliminary estimate of main dimensions. Ocean Eng. 133, 253–261. https://doi.org/10.1016/j.oceaneng.2017.02.011.

Norsok, 2004. Design of Steel Structures, N-004, 2nd ed. Sslo: Norwegian Technology Standards Institution.

Phoon, K.K., Kulhawy, F.H., 1999. Characterization of geotechnical variability. Can. Geotech. J. 36 (4), 612–624. https://doi.org/10.1139/t99-038.

Pohl, C., 2011. Determination of characteristic soil values by statistical methods. In: Proceedings of the 3rd Int. Symp on Geotechnical Safety and Risk (ed. N. Vogt), Karlsruhe, Germany: Bundesanstalt für Wasserbau; 2011. pp. 427-434.

Rogers, J., 2006. Subsurface exploration using the standard penetration test and the cone penetrometer test. Environ. Eng. Geosci. 12 (2), 161–179. https://doi.org/10.2113/12.2.161.

Salgado, R., Lee, J., 1999. Pile design based on cone penetration test results. FHWA/IN/JTRP-99/8, Purdue University, West Lafayette, IN. https://doi.org/10.5703/1288284313293.

Schwab, C., Todor, R.A., 2006. Karhunen-Loève approximation of random fields by generalized fast multipole methods. J. Comput. Phys. 217 (1), 100–122. https://doi.org/10.1016/j.jcp.2006.01.048.

Spagnoli, G., de Hollanda Cavalcanti Tsuha, C., Oreste, P., MendezSolarte, C.M., 2018. Estimation of uplift capacity and installation power of helical piles in sand for offshore structures. Journal of Waterway. Port, Coastal and Ocean Engineering 144 (6): 04018019. https://doi.org/10.1061/(ASCE)WW.1943-5460.0000471.

Thieken, K., Achmus, M., Lemke, K., 2015. A new static p-y approach for piles with arbitrary dimensions in sand. Geotechnik 38 (4), 267–288. https://doi.org/10.1002/gete.201400036.

Uzielli, M., Lacasse, S., Nadim, F., Phoon, K.K., 2007. Soil variability analysis for geotechnical practice. In: Proceedings of the 2nd International Workshop on Characterisation and Engineering Properties of Natural Soils (eds T. S. Tan, K. K. Phoon, D. W. Hight and S. Leroueil), The Netherlands: Taylor and Francis (CD-ROM), Singapore; 2007. pp. 1653-1752. https://doi.org/10.1201/NOE0415426916.ch3.

Uzielli, M., Mayne, P.W., 2019. Probabilistic assignment of effective friction angles of sands and silty sands using quantile regression. Georisk: Assessment and Management of Risk for Engineered Systems and Geohazards 13(4): 271-275. https://doi.org/10.1080/17499518.2019.1663388.

Uzielli, M., Zei, M., Cassidy, M.J., 2019. Probabilistic assignment of design undrained shear strength using quantile regression. In: Proceedings of the 7th International Symposium on Geotechnical Safety and Risk - ISGSR 2019 (eds J. Ching, D. Q. Li and J. Zhang), Taipei, Taiwan; 2019. pp. 188-193. https://doi.org/10.3850/978-981-11-2725-0-IS15-8-cd.

Vanmarcke, E.H., 1984. Random fields: analysis and synthesis. MIT Press, Cambridge, MA.

Wang, Y., Zhao, T., Hu, Y., Phoon, K.K., 2019. Simulation of random fields with trend from sparse measurements without detrending. J. Eng. Mech., ASCE 145 (2), 04018130. https://doi.org/10.1061/(ASCE)EM.1943-7889.0001560.

Wang, Y., Zhao, T., Phoon, K.K., 2018. Direct simulation of random field samples from sparsely measured geotechnical data with consideration of uncertainty in interpretation. Can. Geotech. J. 55 (6), 862–880. https://doi.org/10.1139/cgj-2017-0254.

Wu, X., Hu, Y., Li, Y., Yang, J., Duan, L., Wang, T., Adcock, T., Jiang, Z., Gao, Z., Lin, Z., Borthwick, A., 2019. Foundations of offshore wind turbines: a review. Renew. Sustain. Energy Rev. 104, 379–393. https://doi.org/10.1016/j.rser.2019.01.012.

Zhang, W., Pan, Y., Bransby, F., 2020. Scale effects during cone penetration in spatially variable clays. Géotechnique 24, 1–3. https://doi.org/10.1680/jgeot.20.P.086.

Zhao, T., Wang, Y., 2020. Non-parametric simulation of non-stationary non-Gaussian 3D random field samples directly from sparse measurements using signal decomposition and Markov Chain Monte Carlo. Reliab. Eng. Syst. Saf. 203, 107087 https://doi.org/10.1016/j.ress.2020.107087.

Zhao, T., Xu, L., Wang, Y., 2020. Fast non-parametric simulation of 2D multi-layer cone penetration test (CPT) data without pre-stratification using Markov Chain Monte Carlo simulation. Eng. Geol. 273, 105670 https://doi.org/10.1016/j.enggeo.2020.105670.

Zhu, H., Zhang, L.M., 2013. Characterizing geotechnical anisotropicspatial variations using random field theory. Can. Geotech. J. 50 (7), 723–734. https://doi.org/10.1139/cgj-2012-0345.